CrystEngComm

ROYAL SOCIETY OF CHEMISTRY

COMMUNICATION

View Article Online
View Journal | View Issue

Cite this: *CrystEngComm*, 2023, **25**, 6132

Received 15th September 2023,
Accepted 20th October 2023

DOI: 10.1039/d3ce00917c

rsc.li/crystengcomm

Synthesis and characterization of two metallo-hydrogen-bonded organic frameworks with diverse structures and properties†

Mi Zhou,[ab] Yujiang Wang,[a] Guoyuan Yuan,[a] Zhanfeng Ju [b] and Daqiang Yuan *[b]

Two metallo-hydrogen-bonded organic frameworks (MHOFs) were synthesized by self-assembling a phosphate complex and a macrocyclic ligand with three peripheral carboxylic acids. The two MHOFs have different hydrogen-bond linkages and structures, depending on whether the phosphate participates in the hydrogen bonding. The various hydrogen-bonded networks result in different thermal stabilities, BET surface areas, and water vapor uptake capacities of the MHOFs. MHOF-PO_4-2, which has more hydrogen bonds and higher porosity, shows better thermal stability and water vapor adsorption than MHOF-PO_4-1. This study demonstrates the possibility of constructing diverse and functional MHOFs based on phosphate complexes.

Hydrogen-bonded organic frameworks (HOFs), an emerging type of crystalline porous material, have demonstrated promising applications in various fields such as catalysis,[1–3] sensing,[4–8] proton conductivity,[9,10] and adsorption.[11–17] The construction of HOFs relies on using functional groups with hydrogen-bonded acceptor and donor properties to create molecular building blocks. However, incorporating multiple different functional groups into a single molecule is challenging and limits the functional and structural diversity of HOFs.[18–30] To overcome this limitation, a subclass of HOFs called metallo-hydrogen-bonded organic frameworks (MHOFs) has been developed.[31–35] MHOFs are constructed from complexes that offer abundant geometric configurations, functional groups, and the possibility of incorporating open metal sites.[36,37]

The tetrahedral anion PO_4^{3-} possesses four oxygen atoms on its vertices, thus providing each oxygen atom with the potential to act as a hydrogen bond acceptor. This anion has been utilized in forming supramolecular self-assemblies through hydrogen bonding owing to its highly symmetrical geometry.[38,39] However, to the best of our knowledge, there have been no reports on HOFs based on PO_4^{3-}. This is likely due to the high charge of PO_4^{3-} and the absence of suitable hydrogen-bond donors.[40,41] Therefore, it is crucial to introduce additional components to overcome these limitations. Notably, pioneering researchers have reported the synthesis of a macrocycle that contains a coordinated pocket capable of securely encapsulating three metal ions, particularly Cu(II) and Zn(II), due to macrocyclic and chelating effects.[42–45]

Additionally, charge-balanced anions are present around the resulting complex.[46,47] Inspired by these studies, we synthesized a macrocyclic ligand (**L**) functionalized with three peripheral carboxylic acids using the synthetic pathway depicted in Scheme 1. In this work, we report MHOFs based on the complexation of the macrocycle, Cu(II) and phosphate.

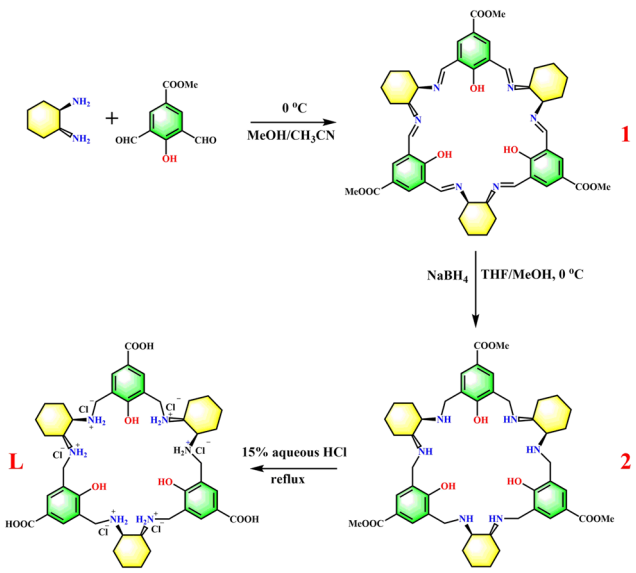

Scheme 1 The synthetic route of L.

[a] *College of Chemistry and Chemical Engineering, Chongqing University of Science and Technology, Chongqing 401331, China*
[b] *State Key Laboratory of Structural Chemistry, Fujian Institute of Research on the Structure of Matter, Chinese Academy of Sciences, Fuzhou 350002, China. E-mail: ydq@fjirsm.ac.cn*

† Electronic supplementary information (ESI) available: Synthesis and X-ray crystallography data in CIF format. CCDC numbers 2286962 and 2287221. For ESI and crystallographic data in CIF or other electronic format see DOI: https://doi.org/10.1039/d3ce00917c

These MHOFs exhibit distinct hydrogen-bond linkages and structures, resulting in significant differences in their BET surface areas, thermal stabilities, and water vapor capacities.

The self-assembly of **L**, $Cu(NO_3)_2$, and K_3PO_4 in H_2O results in the formation of **MHOF-PO$_4$-1**, which is a dark green crystal with a chemical formula $\mathbf{L}Cu_3PO_4{\cdot}6H_2O$. Analysis using single-crystal X-ray diffraction reveals that **MHOF-PO$_4$-1** crystallizes in the space group $F4_132$, with one-third of the formula unit present in the asymmetric unit (Fig. S1a†). Within this complex, three Cu(II) ions adopt a pseudo-square pyramid geometry and are enclosed within the central coordination pocket of **L**. The binding is facilitated by three deprotonated phenol hydroxyls and six secondary amines. Additionally, the three Cu(II) ions are associated with three O atoms from one PO_4^{3-} anion, forming a neutral complex. It is important to note that the PO_4^{3-} ion is located on one side of the complex, while the other remains unoccupied. As a result, the hydrogen atoms of the six secondary amines can be classified into *cis*-groups and *trans*-groups based on their position relative to the PO_4^{3-} ion (Fig. 1a and b).

The bonding between the complex and water molecules leads to the formation of the framework structure of **MHOF-PO$_4$-1**. Each complex is surrounded by six bridging water molecules and three terminal water molecules within this framework. Three of the bridging water molecules form three O–H···O hydrogen bonds with three peripheral carboxylic acids, with an average bond length of 1.847 Å and a bond angle of 162.75°. The other three bridging water molecules form three N–H···O hydrogen bonds with three *trans*-N–H groups, with a bond length of 2.455 Å and a bond angle of 144.94°. Additionally, the three terminal water molecules form three N–H···O hydrogen bonds with three *cis*-N–H groups, with a bond length of 2.252 Å and a bond angle of 160.98° (Fig. 2a). It is important to note that each bridging water molecule simultaneously connects to a carboxylic acid and a *trans*-N–H group from two complexes. In other words, each complex extends to three other complexes through six bridging water molecules, forming a 3-connected hydrogen-bonded network with an *SRS* topology (Fig. 2b and S1b†).

Furthermore, four of these networks interweave through weak intermolecular interactions to create a 4-fold interpenetrated framework (Fig. 2c and d). Within the **MHOF-PO$_4$-1** framework, a pseudo-cuboctahedral cavity is observed, with four complexes occupying four triangular faces (Fig. S1c and d†). **MHOF-PO$_4$-1** is nonporous when analyzed with Zeo^{++} software using a probe radius of 1.86 Å.[48] However, after removing all the water molecules from the framework, a porosity of 19.5% is observed.

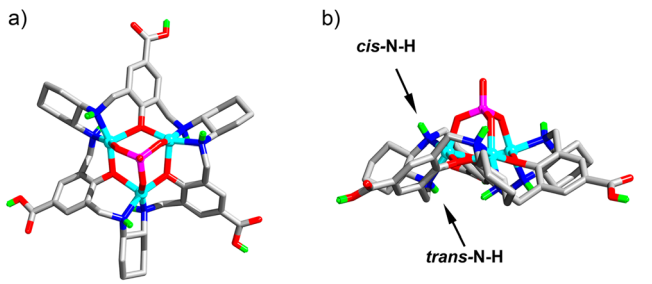

Fig. 1 (a) The structure of the complex; (b) the two kinds of N–H groups in the complex. Purple, sky blue, green, gray, blue, and red spheres represent the P, Cu, H, C, N, and O atoms, respectively.

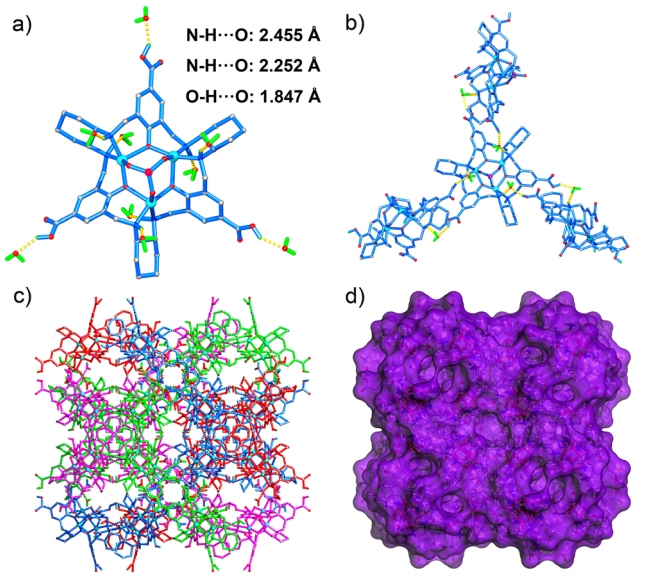

Fig. 2 (a) The hydrogen-bond environment for each complex, (b) the hydrogen-bond linkage between complexes and bridging H_2O, (c) the 4-fold interpenetrated framework, and (d) the channel surface of MHOF-PO$_4$-1.

The analysis indicates that the *cis*-N–H groups, C=O groups of carboxylic acids, and O atoms of phosphate in **MHOF-PO$_4$-1** have minimal contribution to the hydrogen-bond framework. If all potential hydrogen-bond sites are utilized in the framework construction, an MHOF with a stronger hydrogen-bond linkage could be produced. As a result, **MHOF-PO$_4$-2**, which crystallizes in the $P6_3$ space group, was obtained using **MHOF-PO$_4$-1** as the starting material. **MHOF-PO$_4$-2** has the formula $\mathbf{L}Cu_3PO_4{\cdot}3H_2O$, and the asymmetric unit consists of one-third of the formula unit (Fig. S2a†). Structural analysis reveals that the peripheral carboxylic acids of each complex extend outward to three adjacent complexes by forming six hydrogen bonds with three *cis*-N–H groups and three coordinated O atoms of the capped PO_4^{3-}. The distances for O–H···O and N–H···O bonds are approximately 1.669 Å and 2.247 Å, respectively, with bond angles of about 171.68° and 168.53°. Additionally, the three *cis*-N–H groups and three coordinated phosphate O atoms of each complex form six hydrogen bonds with three carboxylic acids from another three complexes simultaneously (Fig. 3a and S2b†). Moreover, edge to face π···π interaction is observed between adjacent complexes (Fig. 3b). Furthermore, the capped PO_4^{3-} forms six hydrogen bonds with three water molecules, with O–H···O distances of approximately 1.883 Å and 2.619 Å and bond angles of about 172.17° and 129.06°. The three hydrogen atoms of the *trans*-N–H groups form three hydrogen bonds with three

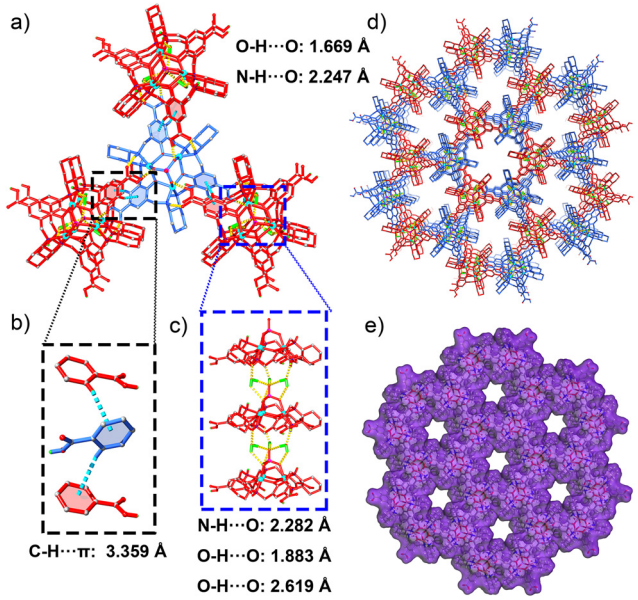

Fig. 3 (a) The hydrogen bonds between complexes, (b) the π···π interaction between adjacent complexes, (c) the inter-complex hydrogen-bond linkage by bridging H_2O, (d) the channel view along the *c* direction, and (e) the channel surface of **MHOF-PO$_4$-2**.

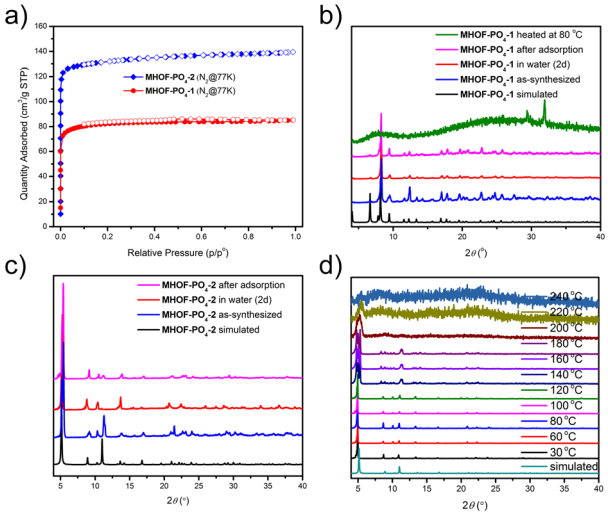

Fig. 4 (a) N_2 (77K) uptake of **MHOF-PO$_4$-1** (red) and **MHOF-PO$_4$-2** (blue); PXRD patterns of (b) **MHOF-PO$_4$-1** and (c) **MHOF-PO$_4$-2**; (d) variable temperature PXRD patterns of **MHOF-PO$_4$-2**.

water molecules, with an average N–H···O distance of 2.282 Å and a bond angle of 138.46°. Consequently, each ligand is connected to two other ligands along the *c* direction through six bridging water molecules, forming a hydrogen-bonded pillar along the *c* direction (Fig. 3c). When calculated using a probe radius of 1.86 Å, **MHOF-PO$_4$-2** exhibits 17.5% porosity and a one-dimensional channel along the *c* direction, with an average pore diameter of 4.96 Å (Fig. 3d and e and S3d†).‡

Based on the analysis above, it is evident that there is a significant variation in the number of hydrogen bonds between **MHOF-PO$_4$-1** and **MHOF-PO$_4$-2**. **MHOF-PO$_4$-2** exhibits more hydrogen bonds, specifically twenty-one, whereas **MHOF-PO$_4$-1** only possesses nine hydrogen bonds (including three terminal bonds). This suggests that **MHOF-PO$_4$-2** maintains a more robust network of hydrogen bonds than **MHOF-PO$_4$-1**. Furthermore, **MHOF-PO$_4$-2** exhibits a higher degree of porosity than **MHOF-PO$_4$-1**, with a calculated probe radius of 1.86 Å, resulting in a porosity of 17.5% for **MHOF-PO$_4$-2**. In contrast, **MHOF-PO$_4$-1** exhibits no porosity at this probe radius.

To analyze the porosity of **MHOF-PO$_4$-1** and **MHOF-PO$_4$-2**, N_2 (77 K) sorption analysis was conducted. Unexpectedly, **MHOF-PO$_4$-1** exhibited a type-I adsorption isotherm with an uptake amount of approximately 85 $cm^3\ g^{-1}$ (Fig. 4a), which contradicts the findings of the structural analysis. Additionally, the crystallinity of **MHOF-PO$_4$-1** remained intact throughout the sorption analysis (Fig. 4b). These abnormal results may be attributed to the loss of select water molecules during activation, with the framework supported by residual hydrogen bonds. On the other hand, **MHOF-PO$_4$-2** exhibited a standard isotherm expected of a microporous material with an uptake amount of around 140 $cm^3\ g^{-1}$. The BET surface area value of **MHOF-PO$_4$-2**, calculated from the experimental N_2 adsorption data, was approximately 520 $m^2\ g^{-1}$.

Furthermore, **MHOF-PO$_4$-2** displayed good crystallinity even after adsorption (Fig. 4c). These findings indicate that **MHOF-PO$_4$-2** possesses a higher BET surface area and N_2 uptake capacity than **MHOF-PO$_4$-1**. However, the two materials exhibited different behaviors when subjected to heat. Specifically, the framework of **MHOF-PO$_4$-1** collapsed when heated to 80 °C (Fig. 4b), whereas **MHOF-PO$_4$-2** maintained its crystallinity up to 120 °C based on variable temperature PXRD analysis (Fig. 4d). Upon heating to higher temperatures, new peaks were observed between 9 and 15°, indicating the formation of a new phase within the bulk sample. Finally, when heated to 200 °C, the sample completely lost its crystallinity, likely due to the breakage of the H-bond linkage. These results are consistent with the findings of the TGA analysis (Fig. S5b†).

Water adsorption is an increasingly popular application for porous materials.[49,50] However, research on this topic is scarce regarding HOFs. Due to the excellent stability of **MHOF-PO$_4$-1** and **MHOF-PO$_4$-2** in water (Fig. 4b and c), water-vapor adsorption experiments were conducted at a temperature of 298 K. The results indicate that **MHOF-PO$_4$-1** only has a water vapor adsorption capacity of 0.003 g g^{-1} (0.176 mmol g^{-1}) (Fig. 5a and S6a†), which can be attributed to its limited pore size and porosity. On the other hand, **MHOF-PO$_4$-2** exhibits a type-IV adsorption isotherm and a total water adsorption amount of 0.254 g g^{-1} (14.1 mmol g^{-1}) (Fig. 5a). The rapid uptake observed at low relative pressures (0 to 0.98 mbar) can be attributed to monolayer adsorption in the channel of **MHOF-PO$_4$-2**. Moreover, the isotherm shows a significant increase in water uptake from 12.92 to 16.94 mbar, suggesting pore-filling progression. Although a hysteresis cycle is observed in the isotherm, the water

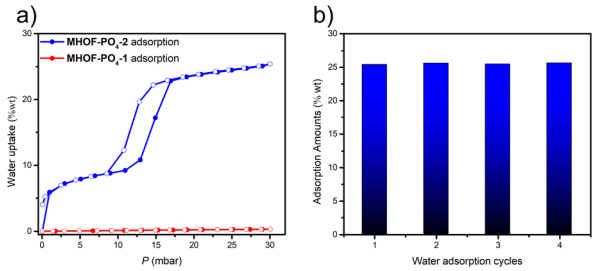

Fig. 5 (a) Water vapor uptake (298 K) of **MHOF-PO$_4$-1** (red) and **MHOF-PO$_4$-2** (blue); (b) water adsorption–desorption (298 K) cycling of **MHOF-PO$_4$-2**.

adsorption capacity of **MHOF-PO$_4$-2** remains reversible. Additionally, the uptake capacity remains almost unchanged after four adsorption and desorption cycles (Fig. 5b and S6†).

Conclusions

We have successfully synthesized two MHOFs based on a phosphate complex and a macrocyclic ligand. The two MHOFs show different hydrogen-bond linkages and structures, which affect their thermal stabilities, BET surface areas, and water vapor uptake capacities. **MHOF-PO$_4$-2**, which has more hydrogen bonds and higher porosity, performs better than **MHOF-PO$_4$-1**. This study demonstrates the possibility of constructing diverse and functional MHOFs based on phosphate complexes. It may provide a new strategy for designing HOFs with tunable properties.

Author contributions

M. Z. was responsible for the design, synthesis, and characterization of the compounds. Additionally, he analyzed the crystal structure and collaborated in writing the paper. Y. W. conducted the water vapor uptake experiments and contributed to the article's writing. G. Y. analyzed the data collected from the water-vapor uptake experiments. Z. J. designed the synthetic route for the ligand. D. Y. planned and supervised the research and collaborated in writing the paper. All authors participated in discussions regarding the results and commented on the manuscript.

Conflicts of interest

There are no conflicts to declare.

Acknowledgements

This work was supported by the Natural Science Foundation of Chongqing (CSTB2022BSXM-JCX0138), the Research Foundation of Chongqing University of Science and Technology (ckrc2021028), and the Chongqing Postdoctoral Science Foundation (2010010005168734).

Notes and references

‡ Crystal data for **MHOF-PO$_4$-1**: $C_{45}H_{69}Cu_3N_6O_{19}P$, M = 1219.65, cubic, space group $F4_13$, a = 37.4254(2) Å, V = 52420.3(8) Å^3, Z = 32, T = 100.0(3) K, 15 912 reflections collected, 4330 unique (R_{int} = 0.0387). Final GooF = 0.992, R_1 = 0.0538, wR_2 = 0.1547, R indices based on 3485 reflections with $I > 2s(I)$ (refinement on F^2), 236 parameters, 157 restraints. Lp and adsorption corrections applied, m = 1.904 mm^{-1}. Absolute structure parameter = 0.025(19). Crystal data for **MHOF-PO$_4$-2**: $C_{45}H_{63}Cu_3N_6O_{16}P$, M = 1165.60, hexagonal, space group $P6_3$, $a = b$ = 19.7940(2) Å, c = 9.02850(10) Å, V = 3063.47(7) Å^3, Z = 2, T = 155(7) K, 22 875 reflections collected, 3924 unique (R_{int} = 0.0228). Final GooF = 1.084, R_1 = 0.0199, wR_2 = 0.0536, R indices based on 3878 reflections with $I > 2s(I)$ (refinement on F^2), 226 parameters, 144 restraints. Lp and adsorption corrections applied, m = 1.977 mm^{-1}. Absolute structure parameter = 0.004(7).

1 Q. Yin, E. V. Alexandrov, D. H. Si, Q. Q. Huang, Z. B. Fang, Y. Zhang, A. A. Zhang, W. K. Qin, Y. L. Li, T. F. Liu and D. M. Proserpio, *Angew. Chem., Int. Ed.*, 2022, **61**, e202115854.
2 K. Ma, P. Li, J. H. Xin, Y. Chen, Z. Chen, S. Goswami, X. Liu, S. Kato, H. Chen, X. Zhang, J. Bai, M. C. Wasson, R. R. Maldonado, R. Q. Snurr and O. K. Farha, *Cell Rep. Phys. Sci.*, 2020, **1**, 100024.
3 R. Azizi, M. Shamsipur, A. Taherpour and A. Pashabadi, *J. Mater. Chem. A*, 2023, **11**, 1491–1502.
4 Q. Huang, W. Li, Z. Mao, H. Zhang, Y. Li, D. Ma, H. Wu, J. Zhao, Z. Yang, Y. Zhang, L. Gong, M. P. Aldred and Z. Chi, *Chem*, 2021, **7**, 1321–1332.
5 B. Wang, R. He, L.-H. Xie, Z.-J. Lin, X. Zhang, J. Wang, H. Huang, Z. Zhang, K. S. Schanze, J. Zhang, S. Xiang and B. Chen, *J. Am. Chem. Soc.*, 2020, **142**, 12478–12485.
6 W. Jiang, H. Zheng, Y. Wu, P. Wu, L. Jing, X. Yuan, X. Wang and J. Wang, *Inorg. Chem. Front.*, 2023, **10**, 5430–5438.
7 C. Yang, X. Xu and B. Yan, *Inorg. Chem. Front.*, 2023, **10**, 2951–2960.
8 Q. Huang, W. Li, Z. Yang, J. Zhao, Y. Li, Z. Mao, Z. Yang, S. Liu, Y. Zhang and Z. Chi, *CCS Chem.*, 2022, **4**, 1643–1653.
9 E. A. Zhigileva, Y. Y. Enakieva, A. A. Sinelshchikova, V. V. Chernyshev, I. N. Senchikhin, K. A. Kovalenko, I. A. Stenina, A. B. Yaroslavtsev, Y. G. Gorbunova and A. Y. Tsivadze, *Dalton Trans.*, 2023, **52**, 8237–8246.
10 Q. Yang, X. Li, C. Xie, Z. Wang, Z. Kong, J. Yang, Z. Kang, R. Wang and D. Sun, *J. Mater. Chem. C*, 2023, **11**, 12206–12212.
11 F. Hu, C. Liu, M. Wu, J. Pang, F. Jiang, D. Yuan and M. Hong, *Angew. Chem., Int. Ed.*, 2017, **56**, 2101–2104.
12 B. Yu, S. Geng, H. Wang, W. Zhou, Z. Zhang, B. Chen and J. Jiang, *Angew. Chem., Int. Ed.*, 2021, **60**, 25942–25948.
13 B. Wang, R.-B. Lin, Z. Zhang, S. Xiang and B. Chen, *J. Am. Chem. Soc.*, 2020, **142**, 14399–14416.
14 B. Wang, X.-L. Lv, J. Lv, L. Ma, R.-B. Lin, H. Cui, J. Zhang, Z. Zhang, S. Xiang and B. Chen, *Chem. Commun.*, 2020, **56**, 66–69.
15 D.-D. Zhou, Y.-T. Xu, R.-B. Lin, Z.-W. Mo, W.-X. Zhang and J.-P. Zhang, *Chem. Commun.*, 2016, **52**, 4991–4994.
16 Y. Zhou, L. Kan, J. F. Eubank, G. Li, L. Zhang and Y. Liu, *Chem. Sci.*, 2019, **10**, 6565–6571.
17 Y. Liu, J. Dai, L. Guo, Z. Zhang, Y. Yang, Q. Yang, Q. Ren and Z. Bao, *CCS Chem.*, 2022, **4**, 381–388.

18 C.-F. Ng, H.-F. Chow and T. C. W. Mak, *Cryst. Growth Des.*, 2022, **22**, 3365–3375.
19 F. Haase, G. A. Craig, M. Bonneau, K. Sugimoto and S. Furukawa, *J. Am. Chem. Soc.*, 2020, **142**, 13839–13845.
20 Y. Zhao, C. Fan, C. Pei, X. Geng, G. Xing, T. Ben and S. Qiu, *J. Am. Chem. Soc.*, 2020, **142**, 3593–3599.
21 T. Khadivjam, H. Che-Quang, T. Maris, Z. Ajoyan, A. J. Howarth and J. D. Wuest, *Chem. – Eur. J.*, 2020, **26**, 7026–7040.
22 Y. Li, M. Handke, Y.-S. Chen, A. G. Shtukenberg, C. T. Hu and M. D. Ward, *J. Am. Chem. Soc.*, 2018, **140**, 12915–12921.
23 T. Hashimoto, R. Oketani, A. Inoue, K. Okubo, K. Oka, N. Tohnai, K. Kamiya, S. Nakanishi and I. Hisaki, *Chem. Commun.*, 2023, **59**, 7224–7227.
24 J.-Q. Zhao, L.-L. Mao, G.-H. Zhang, S.-Z. Zhan, H. Xiao, S. Zhang, C.-H. Tung, L.-Z. Wu and H. Cong, *J. Mater. Chem. A*, 2023, **11**, 4672–4678.
25 T. H. Chen, I. Popov, W. Kaveevivitchai, Y. C. Chuang, Y. S. Chen, O. Daugulis, A. J. Jacobson and O. S. Miljanic, *Nat. Commun.*, 2014, **5**, 5131.
26 A. Pulido, L. Chen, T. Kaczorowski, D. Holden, M. A. Little, S. Y. Chong, B. J. Slater, D. P. McMahon, B. Bonillo, C. J. Stackhouse, A. Stephenson, C. M. Kane, R. Clowes, T. Hasell, A. I. Cooper and G. M. Day, *Nature*, 2017, **543**, 657–664.
27 G. Xing, I. Bassanetti, S. Bracco, M. Negroni, C. Bezuidenhout, T. Ben, P. Sozzani and A. Comotti, *Chem. Sci.*, 2019, **10**, 730–736.
28 J. Lü, C. Perez-Krap, F. Trousselet, Y. Yan, N. H. Alsmail, B. Karadeniz, N. M. Jacques, W. Lewis, A. J. Blake, F.-X. Coudert, R. Cao and M. Schröder, *Cryst. Growth Des.*, 2018, **18**, 2555–2562.
29 J. Sun, H.-X. Liu and T.-F. Liu, *Chin. J. Struct. Chem.*, 2021, **40**, 1082–1087.
30 P. Liu, A. Liu, P. Wang, Y. Chen and B. Li, *Chin. J. Struct. Chem.*, 2023, **42**, 100001.
31 H.-L. Wang, X.-F. Ma, Z.-H. Zhu, Y.-Q. Zhang, H.-H. Zou and F.-P. Liang, *Inorg. Chem. Front.*, 2019, **6**, 2906–2913.
32 S. Chand, S. C. Pal, A. Pal, Y. Ye, Q. Lin, Z. Zhang, S. Xiang and M. C. Das, *Chem. – Eur. J.*, 2019, **25**, 1691–1695.
33 Z. Ju, G. Liu, Y. S. Chen, D. Yuan and B. Chen, *Chem. – Eur. J.*, 2017, **23**, 4774–4777.
34 R. B. Lin, Y. He, P. Li, H. Wang, W. Zhou and B. Chen, *Chem. Soc. Rev.*, 2019, **48**, 1362–1389.
35 Z. Bao, D. Xie, G. Chang, H. Wu, L. Li, W. Zhou, H. Wang, Z. Zhang, H. Xing, Q. Yang, M. J. Zaworotko, Q. Ren and B. Chen, *J. Am. Chem. Soc.*, 2018, **140**, 4596–4603.
36 M. Zhou, G. Liu, Z. Ju, K. Su, S. Du, Y. Tan and D. Yuan, *Cryst. Growth Des.*, 2020, **20**, 4127–4134.
37 U. Yamashita, N. Yoshinari, R. Sodkhomkhum, N. Meundaeng and T. Konno, *CrystEngComm*, 2020, **22**, 2700–2704.
38 B. Li, B. Zheng, W. Zhang, D. Zhang, X.-J. Yang and B. Wu, *J. Am. Chem. Soc.*, 2020, **142**, 6304–6311.
39 T. S. C. MacDonald, B. L. Feringa, W. S. Price, S. J. Wezenberg and J. E. Beves, *J. Am. Chem. Soc.*, 2020, **142**, 20014–20020.
40 R. S. Voguri, S. Ranga, A. Dey and S. Ghosal, *Cryst. Growth Des.*, 2020, **20**, 7647–7657.
41 W. Gong, D. Chu, H. Jiang, X. Chen, Y. Cui and Y. Liu, *Nat. Commun.*, 2019, **10**, 600.
42 M. Petryk, A. Janiak, L. J. Barbour and M. Kwit, *Eur. J. Org. Chem.*, 2018, **2018**, 1916–1923.
43 S. Y. Lin, Y. N. Guo, Y. Guo, L. Zhao, P. Zhang, H. Ke and J. Tang, *Chem. Commun.*, 2012, **48**, 6924–6926.
44 J. Gao, R. A. Zingaro, J. H. Reibenspies and A. E. Martell, *Org. Lett.*, 2004, **6**, 2453–2455.
45 S. R. Korupoju, N. Mangayarkarasi, P. S. Zacharias, J. Mizuthani and H. Nishihara, *Inorg. Chem.*, 2002, **41**, 4099–4101.
46 S. Y. Lin, C. Wang, L. Zhao, J. Wu and J. Tang, *Dalton Trans.*, 2015, **44**, 223–229.
47 Z. Chu, W. Huang, L. Wang and S. Gou, *Polyhedron*, 2008, **27**, 1079–1092.
48 T. F. Willems, C. H. Rycroft, M. Kazi, J. C. Meza and M. Haranczyk, *Microporous Mesoporous Mater.*, 2012, **149**, 134–141.
49 Z. Zheng, N. Hanikel, H. Lyu and O. M. Yaghi, *J. Am. Chem. Soc.*, 2022, **144**, 22669–22675.
50 N. Hanikel, X. Pei, S. Chheda, H. Lyu, W. Jeong, J. Sauer, L. Gagliardi and O. M. Yaghi, *Science*, 2021, **374**, 454–459.

